Engineering Structures 255 (2022) 113911

Contents lists available at ScienceDirect

Engineering Structures

journal homepage: www.elsevier.com/locate/engstruct

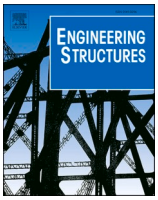

Scale effects in prestressed concrete structures: Maximum reinforcement percentage to avoid brittle crushing

Alberto Carpinteri [a,b], Federico Accornero [a,*], Renato Cafarelli [a]

[a] Dept of Structural, Geotechnical and Building Engineering, Politecnico di Torino, Torino, Italy
[b] Zhujiang (Pearl River) Professor of Guangdong Province, Dept of Civil and Environmental Engineering, Shantou University, Shantou, China

ARTICLE INFO

Keywords:
Prestressed concrete
Fracture mechanics
Scale effects
Ductile-to-brittle transition
Concrete crushing

ABSTRACT

The structural behaviour of prestressed concrete beams is considerably affected by different nonlinear phenomena occurring in post-cracking and crushing regimes, such as snap-back or snap-through instabilities. Design procedures included in current technical Standards are not able to take into account the actual crushing regime, since the adopted constitutive laws overlook the strain-localization and softening behaviour of the concrete matrix. Moreover, design provisions are usually based on Plasticity Theory, leading to completely disregard size-scale effects and ductile-to-brittle transitions as functions of the beam depth.

In the present paper, the above-mentioned shortcomings are overtaken by means of a Fracture Mechanics approach. The Cohesive/Overlapping Crack Model is able to simulate the strain-localization and softening regime of concrete both in tension and compression, predicting the nonlinear crushing behaviour of prestressed concrete beams. Then, a scale-dependent maximum reinforcement percentage formulation is provided in order to avoid concrete crushing failure. In this way, the field in which prestressed concrete structures can develop a safe ductile behavior can be defined, formulating new standard requirements for an effective structural design.

1. Introduction

The structural behaviour of quasi-brittle materials is heavily influenced by specimen dimensions and loading conditions [1]. In this framework, the cracking load has been regarded as a discontinuity condition for the equilibrium path, since post-peaking branches could be described by means of a non-single slope in the load vs deflection diagram. As a matter of fact, for large size, high strength, and/or low toughness specimens, a snap-back phenomenon could be detected in the softening regime [2]. Snap-back represents a catastrophic condition for the structural system since it implies a decrease in the load-carrying capacity, as well as in the deflection. This unstable branch could be revealed experimentally only if a monotonic increasing function of time, such as the crack mouth opening displacement, is adopted as controlling variable [3,4]. Size-scale effects in concrete and, more generally, in concrete-like materials are always expected due to the different physical dimensions between strength σ_t [FL^{-2}] and fracture energy [FL^{-1}], as suggested in [5]. Size-scale effects have been observed experimentally in reinforced concrete (RC) and prestressed concrete (PC) beams failing in flexure [6], shear [7–9], or compression [10,11]. In the past few years, each failure mechanism has been investigated independently from the others, leading to models that are not able to thoroughly predict the transitions between different failure modes [12,13], which are function of beam depth, h, slenderness, λ, and reinforcement percentage, ρ. In the past few years, size-scale effects in over-reinforced concrete beams have been addressed by means of a scale-dependent formulation for determining the effective concrete compressive strength [14,15]. Nevertheless, such an approach is not able to thoroughly predict the ductile-to-brittle transitions of prestressed concrete structures since it neglects the parameters related to the reinforcement together with the effects of the stress gradient generated by a possible prestressing force.

The strain-softening behaviour of concrete in tension has been widely studied in the past decades [16–20] and many models have been proposed to predict the ductile-to-brittle transition of plain concrete specimens. On the other hand, only in 1997 the round-robin organized by RILEM TC 148-SSC [21] evidenced that an actual constitutive law for concrete in compression should be identified in a σ-w^c diagram, being w^c an inelastic displacement, rather than in the usual σ-ε diagram. As an example, in Fig. 1 the experimental tests carried out by Ferrara and Gobbi [22] at ENEL-CRIS laboratory in Milan (Italy) are reported. The tests were performed on concrete prisms having different dimensions: 50 × 50 mm (S), 100 × 100 mm (M) and 150 × 150 mm (L) and three slenderness ratios (0.5, 1.0, 2.0). The results of this campaign are

* Corresponding author.
E-mail address: federico.accornero@polito.it (F. Accornero).

https://doi.org/10.1016/j.engstruct.2022.113911
Received 29 July 2021; Received in revised form 25 December 2021; Accepted 15 January 2022
Available online 3 February 2022

Nomenclature

σ_t	tensile strength of concrete;
ε_t	ultimate tensile strain of concrete;
w^t	crack opening;
w^t_{cr}	critical value of crack opening;
G_F	fracture energy;
σ_c	compressive strength of concrete;
ε_c	ultimate compressive strain of concrete;
w^c	fictitious interpenetration;
w^c_{cr}	critical value of fictitious interpenetration;
G_c	crushing energy;
E	concrete elastic modulus;
σ_p	prestressing steel stress;
n	number of nodes;
$\{w\}$	vector of nodal displacements;
$[K_F]$	matrix of nodal displacements generated by unit forces;
$\{F\}$	vector of nodal forces;
$\{K_M\}$	vector of nodal displacements generated by unit bending moment;
M	bending moment;
$\{F_p\}$	vector of nodal forces generated by prestressing;
h	beam depth;
b	beam thickness;
A_{sp}	prestressing steel area;
ρ_p	prestressing steel reinforcement percentage;
$\rho_{p,max}$	maximum prestressing reinforcement percentage;
σ_y	steel yield strength;
s_c	concrete brittleness number;
N_P^U	critical value of reinforcement brittleness number;
N_p^0	prestressing brittleness number.

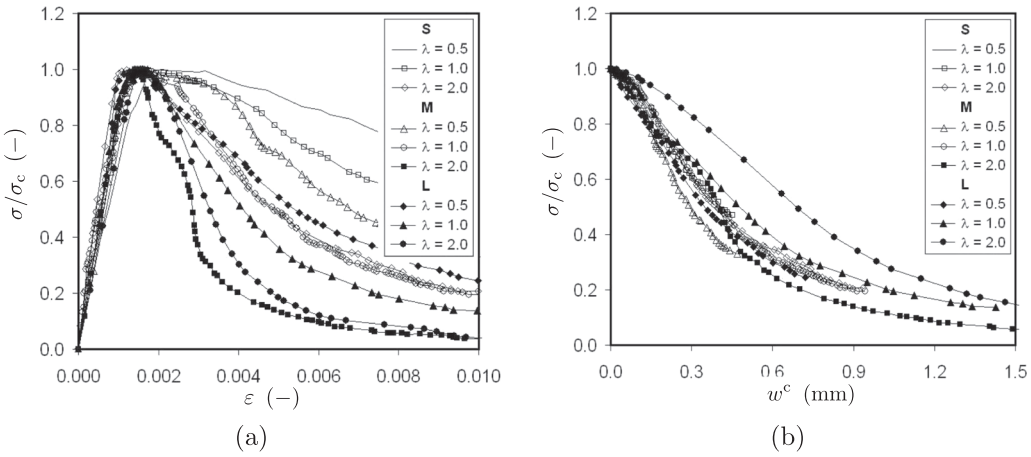

Fig. 1. Uniaxial compression tests [22]: (a) σ/σ_c-ε relationships; (b) post-peak σ/σ_c-w^c relationships.

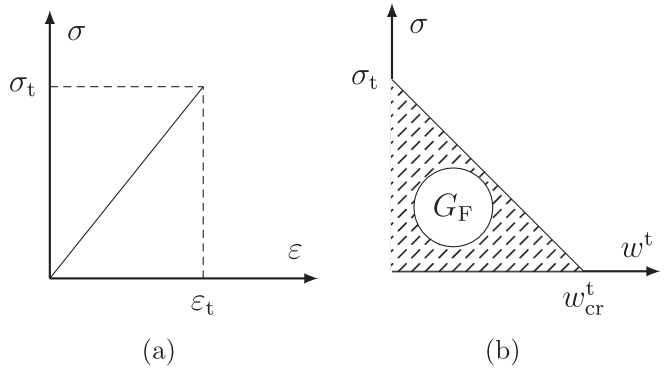

Fig. 2. Cohesive Crack Model: (a) linear-elastic stress–strain law; (b) post-peak σ-w^t cohesive relationship.

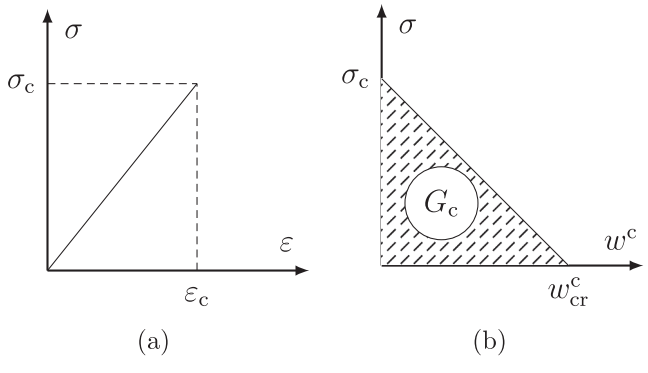

Fig. 3. Overlapping Crack Model: (a) linear elastic stress–strain law; (b) post-peak stress vs. fictitious interpenetration relationship.

collected in a σ-ε diagram in Fig. 1a where a high dependency of post-peak curves with specimen scale and slenderness is acknowledged. On the other hand, if the softening branches are reported in a σ/σ_c-w^c diagram as in Fig. 1b, the curves become almost independent of the specimen size and are restrained within a narrow band. In this framework, Jansen and Shah [23] demonstrated that the area subtended by the σ-w^c curve represents the crushing energy, G_c, a material property independent of the specimen size.

In the present paper, a dimensional approach is adopted to outline the fundamental features governing the crushing failure of PC beams. Thus, the Cohesive/Overlapping Crack Model [24–27] is applied to define a scale-dependent maximum reinforcement ratio, $\rho_{p,max}$, beyond which PC structural elements exhibit an unstable ultimate behaviour, since a compression snap-back immediately after peak load is revealed, removing any plastic-rotation capacity of the PC beam.

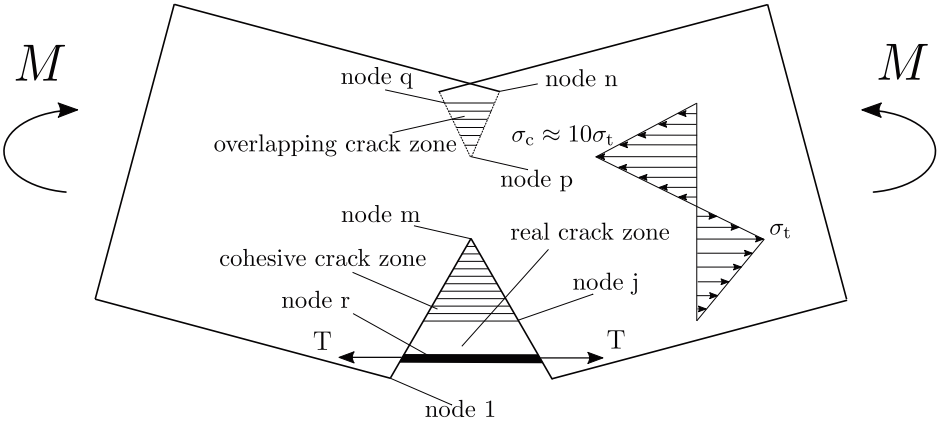

Fig. 4. Cohesive/Overlapping Crack Model.

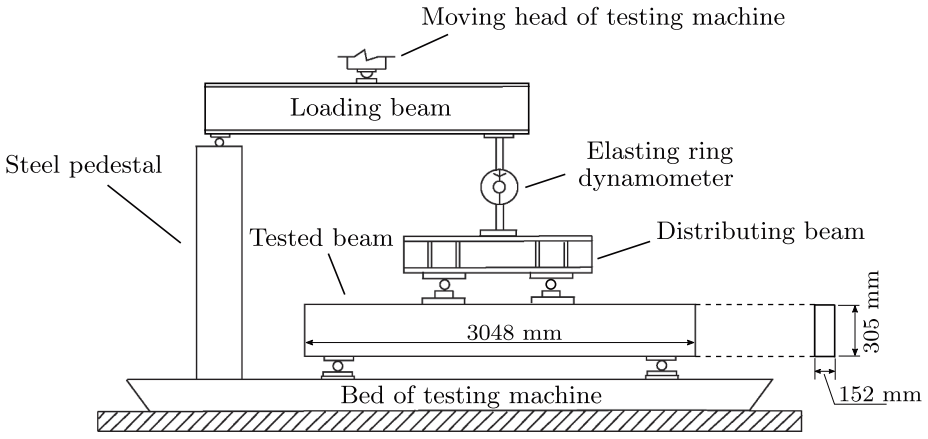

Fig. 5. Testing set-up and beam geometry adopted by Billet [37]

Table 1
PC beams tested in [37] and their failure modes (T = Cracking; C = Crushing; S = Shearing; B = Bond failure).

Beam	σ_c (MPa)	d (mm)	A_s (mm^2)	σ_p (MPa)	σ_y (MPa)	E (MPa)	σ_t (MPa)	G_F (N/mm)	G_c (N/mm)	Failure mode
B1	37.8	231	159	823	1560	—	3.4	0.145	30	B
B2	33.5	242	75	828	1560	22,621	3.1	0.143	30	T
B3	27.4	244	37	834	1560	23,380	2.7	0.139	30	T
B4	26.3	233	150	841	1560	35,172	2.7	0.138	30	T-S
B5	41.1	237	161	823	1570	21,241	3.6	0.147	31	T-S
B6	22.1	206	221	832	1570	33,103	2.4	0.135	30	C-S
B7	37.4	205	301	815	1570	21,586	3.4	0.145	30	C
B8	23.3	203	301	838	1570	25,517	2.4	0.136	30	C
B9	41.8	234	151	141	1550	33,379	3.6	0.148	32	T
B10	23.7	229	38	148	1550	21,586	2.5	0.136	30	T
B11	25.7	234	151	144	1550	25,517	2.6	0.137	30	T-C
B12	39.1	212	283	140	1550	33,379	3.5	0.146	30	C-B
B13	27.8	207	208	154	1550	30,759	2.8	0.139	30	C
B14	28.2	203	283	143	1550	29,379	2.8	0.139	30	C
B15	39.6	236	151	1034	1550	33,035	3.5	0.146	30	T
B16	22.2	229	38	1037	1550	24,621	2.4	0.135	30	T
B17	29.2	231	151	1041	1550	30,621	2.8	0.140	30	T
B18	26.9	211	208	1026	1550	30,966	2.7	0.138	30	T-C
B19	41.2	210	283	1043	1550	32,000	3.6	0.147	31	T-C
B20	22.9	235	101	830	1570	27,241	2.4	0.135	30	B
B21	44.6	230	101	834	1570	36,345	3.8	0.149	35	T
B22	51.4	232	201	830	1570	41,310	4.1	0.152	41	T
B23	55.7	208	301	836	1570	37,931	4.2	0.154	44	T-C
B24	41.5	209	241	837	1570	36,069	3.6	0.147	32	T-C
B25	19.1	203	201	836	1570	25,586	2.1	0.132	30	C
B26	11.6	235	161	839	1570	14,621	1.5	0.125	30	C
B27	31.6	212	301	839	1570	28,276	3.0	0.142	30	C

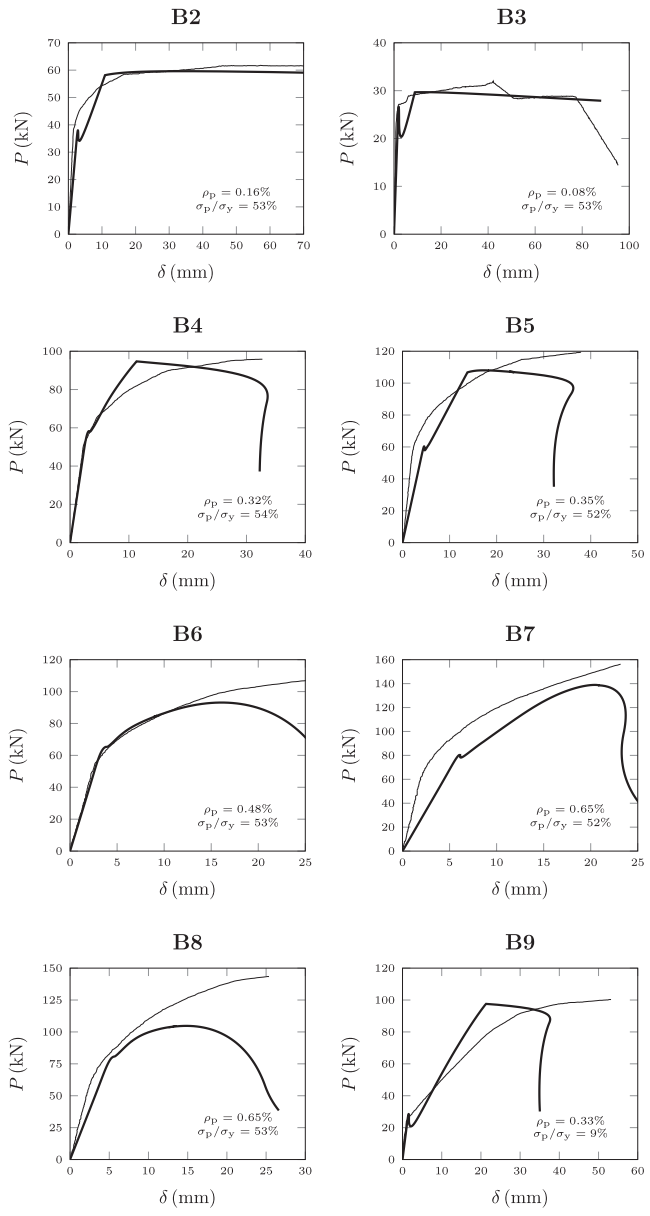

Fig. 6. Numerical (thick) vs. experimental (thin) curves for beams B2-B9.

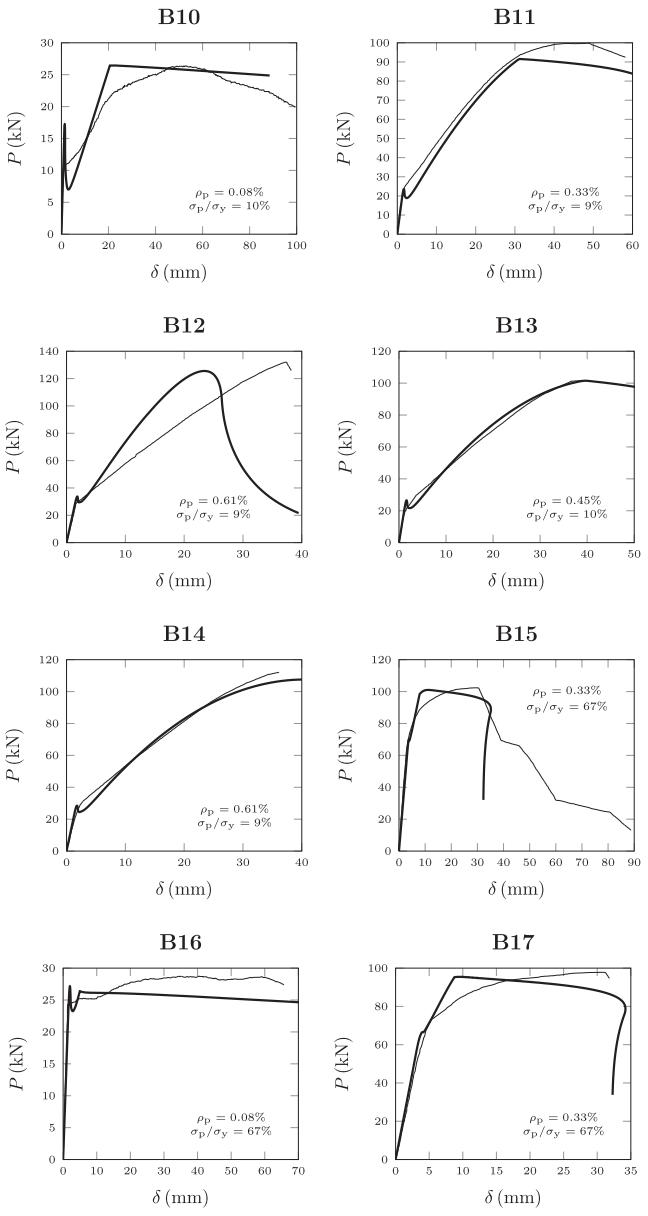

Fig. 7. Numerical (thick) vs. experimental (thin) curves for beams B10-B17.

2. The cohesive/overlapping crack model

The Cohesive Crack Model [1–3,28–30] has been adopted as a powerful tool in the investigation of the ductile-to-brittle transition occurring in concrete elements as a function of structural size, h, material tensile strength, σ_t, and fracture energy, G_F. The beahviour of the undamaged material is represented by means of a linear elastic constitutive law, which is defined in the σ-ε diagram (Fig. 2a). On the other hand, in the zone where strain localization occurs, a constitutive law can be defined in the σ-w^t diagram (Fig. 2b), being w^t the crack opening displacement. The area subtended by the σ-w^t curve represents the fracture energy, G_F, which is an actual material property independent of the beam depth [31].

On the other hand, the Overlapping Crack Model [32] was introduced in order to simulate the compressive damage of concrete occurring at the beam extrados. In close analogy to the Cohesive Crack Model, the Overlapping Crack Model assumes two constitutive laws for concrete in compression: the behaviour of the undamaged material is modelled in the σ-ε diagram (Fig. 3a), whereas a constitutive law defined in a σ-w^c diagram is used in the damaged zone (Fig. 3b), w^c being an overlapping displacement discontinuity representing strain localization in compression and possible extreme phenomena of ejection. The area subtended by the σ-w^c curve is the crushing energy, G_c, which presents the same physical dimensions as the fracture energy G_F [21,23].

In the Cohesive/Overlapping Crack Model [24–27], the two above-mentioned constitutive laws are integrated in order to take into account the concrete nonlinear behaviour both in tension and in compression. Due to its characteristics, this Fracture Mechanics model is particularly suitable in the investigation of over-reinforced or pre-stressed concrete beams, since matrix crushing represents in these cases the dominant phenomenon in the post-cracking regime [10,11,25].

Within the Cohesive/Overlapping Crack Model, the beam cross-section is divided into n nodes (Fig. 4), for which the following linear elastic equation can be written:

$$\{w\} = [K_F]\{F\} + \{K_M\}M + [K_F]\{F_p\} \tag{1}$$

where $\{w\}$ is the vector of the opening/overlapping displacements; $[K_F]$ is the matrix containing the nodal displacements generated by unit nodal forces; $\{F\}$ is the vector of nodal forces; $\{K_M\}$ is the vector

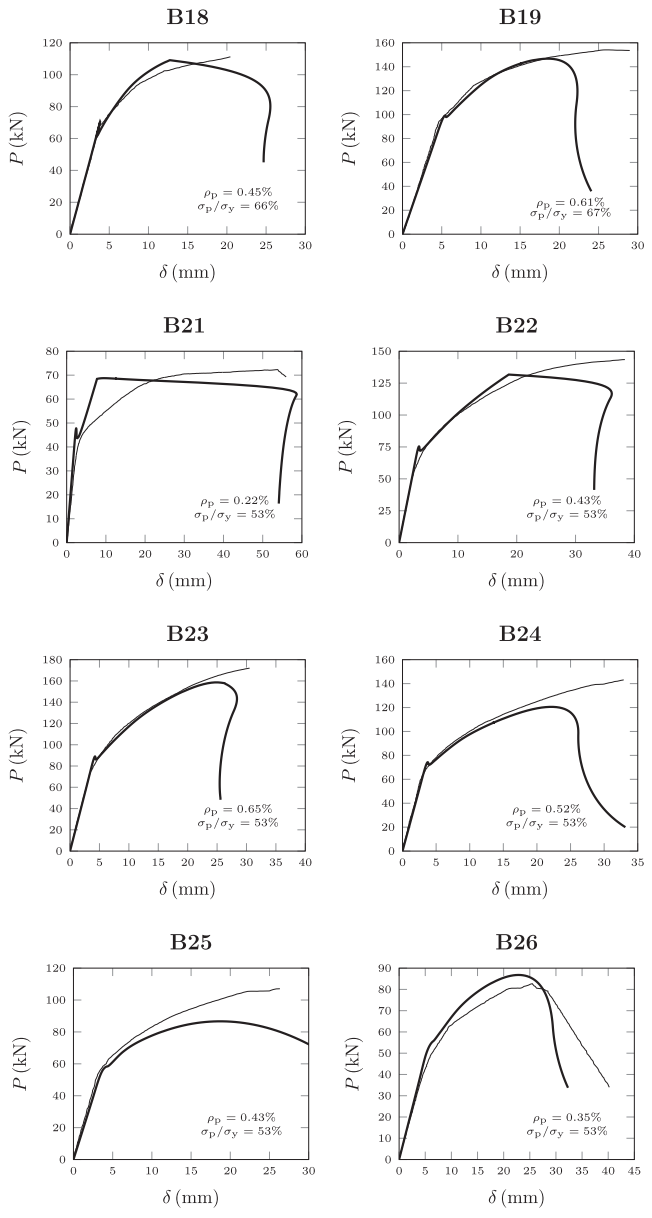

Fig. 8. Numerical (thick) vs. experimental (thin) curves for beams B18-B26.

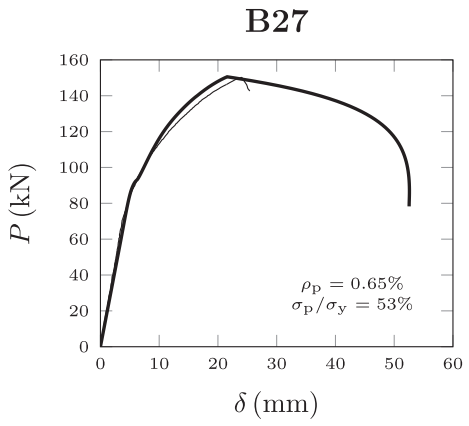

Fig. 9. Numerical (thick) vs. experimental (thin) curves for beam B27.

containing the nodal displacements generated by a unit bending moment; M is the applied bending moment; $\{F_p\}$ is the vector containing the nodal forces generated by an eventual prestressing force. The unknowns involved in Eq. (1) are $(2n + 1)$ and have both static and kinematic nature. In the general case of Fig. 4, it is possible to consider the following conditions (Fig. 2b and Fig. 3b):

$$F_i = 0 \quad \text{for} \quad i = 1, ..., (j-1), \; i \neq r \tag{2a}$$

$$F_i = F_t\left(1 - \frac{w_i}{w_{cr}^t}\right) \quad \text{for } i = j, ..., (m-1) \tag{2b}$$

$$w_i = 0 \quad \text{for } i = m, ..., p \tag{2c}$$

$$F_i = F_c\left(1 - \frac{w_i}{w_{cr}^c}\right) \quad \text{for } i = (p+1), ..., q \tag{2d}$$

$$F_i = 0 \quad \text{for } i = (q+1), ..., n \tag{2e}$$

$$F_i = f(w_i) \quad \text{for } i = r \tag{2f}$$

where j is the real cohesive crack tip; m is the fictitious cohesive crack tip; p is the fictitious overlapping zone tip; q is the real overlapping zone tip. Eq. (2f) represents a constitutive law for the steel strand in the form σ-w^t, which is calibrated following Model Code 2010 [30,33] as reported in detail in [25]. The conditions involved in Eq. (2) reduce the unknowns of Eq. (1). Thus, the value of M is assumed as the minimum load that generates the ultimate tensile force, F_t, or the ultimate compressive force, F_c, in node m or p, respectively.

3. Numerical vs. Experimental investigations

In this section, a numerical vs. experimental comparison will be proposed in order to validate the capability of the Cohesive/Overlapping Crack Model in predicting the post-cracking behaviour of PC beams. In the scientific literature, there are few experimental campaigns investigating the post-cracking flexural behaviour of PC beams [34–36,25]. In the present paper, the experimental campaign carried out by Billet [37] in collaboration with the American Bureau of Public Roads is considered. This campaign involves 27 specimens and was planned to investigate the failure modes of post-tensioned bonded PC beams by varying the prestressing steel ratio, $\rho_p = A_s/(hb)$, and the prestressing level, σ_p/σ_y. The four-point bending tests were performed on beams having a cross-section 152 × 305 mm and a span equal to 3048 mm, as reported in Fig. 5. No reinforcement was placed in the compression region of the beams and stirrups were provided only near the bearings in order to avoid shearing failure. Moreover, the tests were carried out using a load-control system until slight crushing or excessive steel elongation occurred. Since in this case the load is not a monotonically increasing function of time, unstable snap-back or snap-through branches could not be followed in a stable manner during the tests [3,4]. The detailed geometrical and mechanical parameters of the tested beams, together with their failure modes, are reported in Table 1. It is worth noting that, since beams B1 and B20 experienced bond failure, they have been excluded from the numerical vs. experimental comparison presented in the following. Moreover, concrete tensile strength, σ_t, and fracture energy, G_F, were determined according to the Model Code 2010 [33]. On the other hand, the crushing energy, G_c, was calculated applying the formula by Suzuki [38].

In Fig. 6, a numerical (thick curve) vs. experimental (thin curve) comparison for PC beams B2 to B9 is presented. It is possible to observe that the Cohesive/Overlapping Crack Model is able to describe accurately the post-cracking nonlinear behaviour: snap-back due to concrete cracking, steel yielding, and snap-back due to concrete crushing can be thoroughly predicted. Furthermore, Figs. 6 and 7 outline a ductile-to-brittle transition increasing the prestressing reinforcement ratio, ρ_p: for $\sigma_p/\sigma_y = 53\%$, it is possible to observe a migration from cracking to

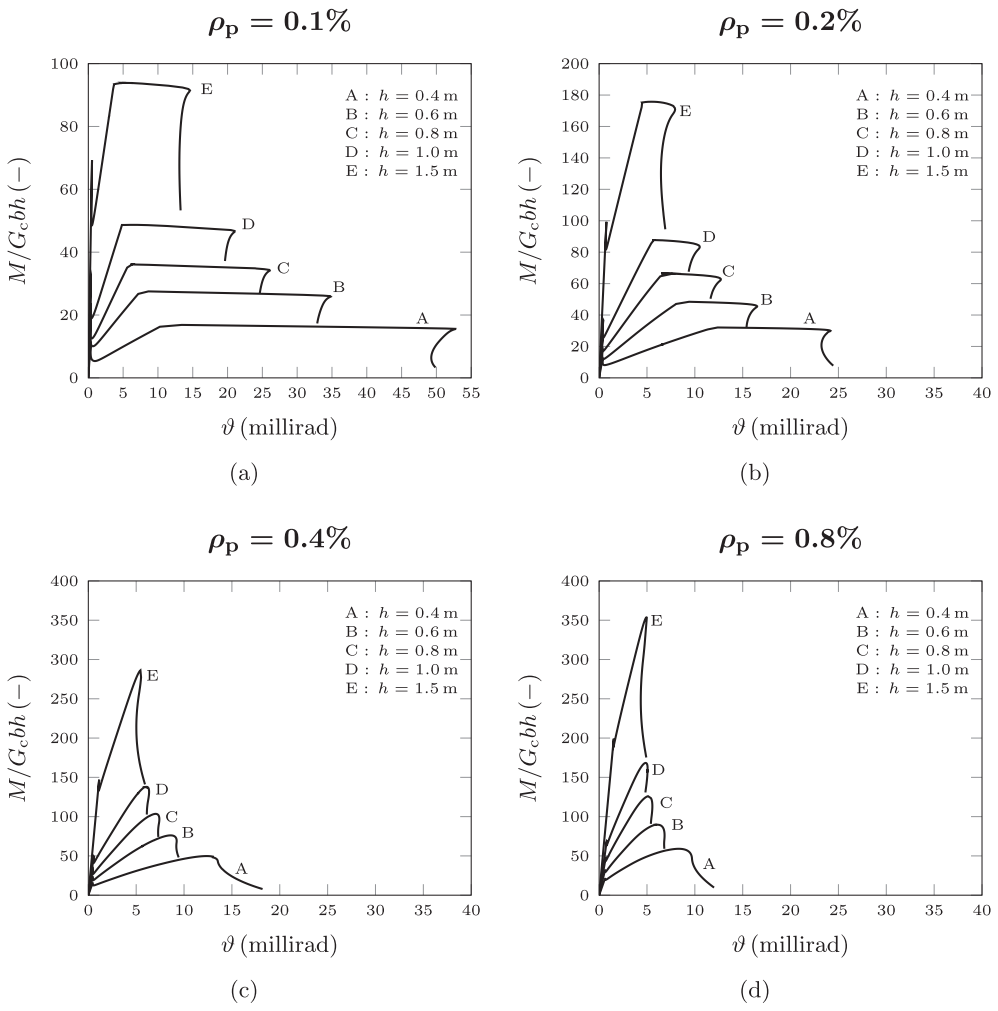

Fig. 10. Nondimensional load vs. rotation curves for. (a) $\rho_p = 0.1\%$; (b) $\rho_p = 0.2\%$; (c) $\rho_p = 0.4\%$; (d) $\rho_p = 0.8\%$

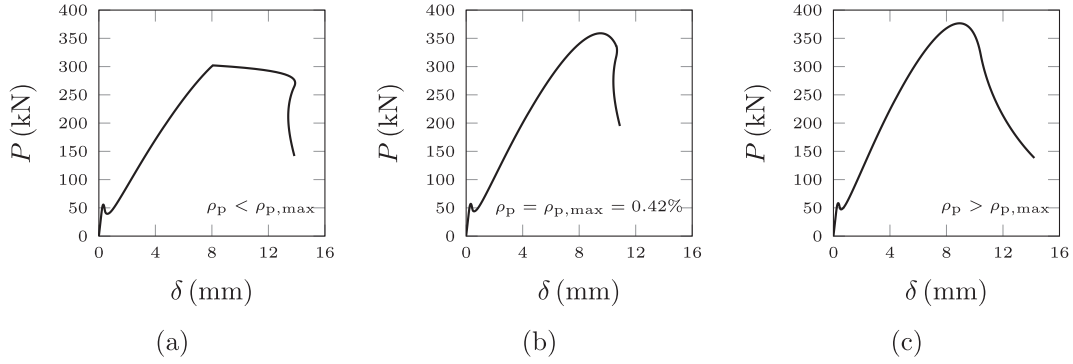

Fig. 11. Ductile-to-brittle transition for $N_p{}^0 = 0.05$ and $s_c = 1.58$: (a) stable behaviour; (b) balanced reinforcement condition; (c) unstable behaviour.

crushing failure (specimens B2; B4; B5; B6; B7), together with a progressive decrement in the extension of the plastic plateau as ρ_p increases. In Figs. 8 and 9, the PC beams present a flexural behaviour strongly conditioned by concrete crushing. For these specimens, the load-carrying capacity is limited by concrete ultimate behaviour: steel yielding does not occur (except for B18, B21, B22) and a catastrophic failure occurs due to unstable propagation of the crushing zone at the beam extrados.

Figs. 6-9 suggest that the Cohesive/Overlapping Crack Model presents a high capability in the prediction of PC beam post-cracking and post-crushing behaviour, together with the transition from ductile (flexural) to brittle (crushing) failure increasing the prestressing steel ratio, ρ_p.

Unfortunately, the wide experimental campaign carried out by Billet [37] does not take into account any variation in beam size.

In order to recover this lack in terms of size-scale effect, a numerical study is performed by means of the Cohesive/Overlapping Crack Model to investigate the influence of the beam depth, h, on the plastic rotation capacity developed by PC beams. This numerical investigation ranges over five different beam depths, h, and four different prestressing reinforcement percentages, ρ_p. A prestressing force equal to $1/3\ \sigma_y A_{sp}$, being A_{sp} the prestressing steel-strand area, is considered for all the specimens.

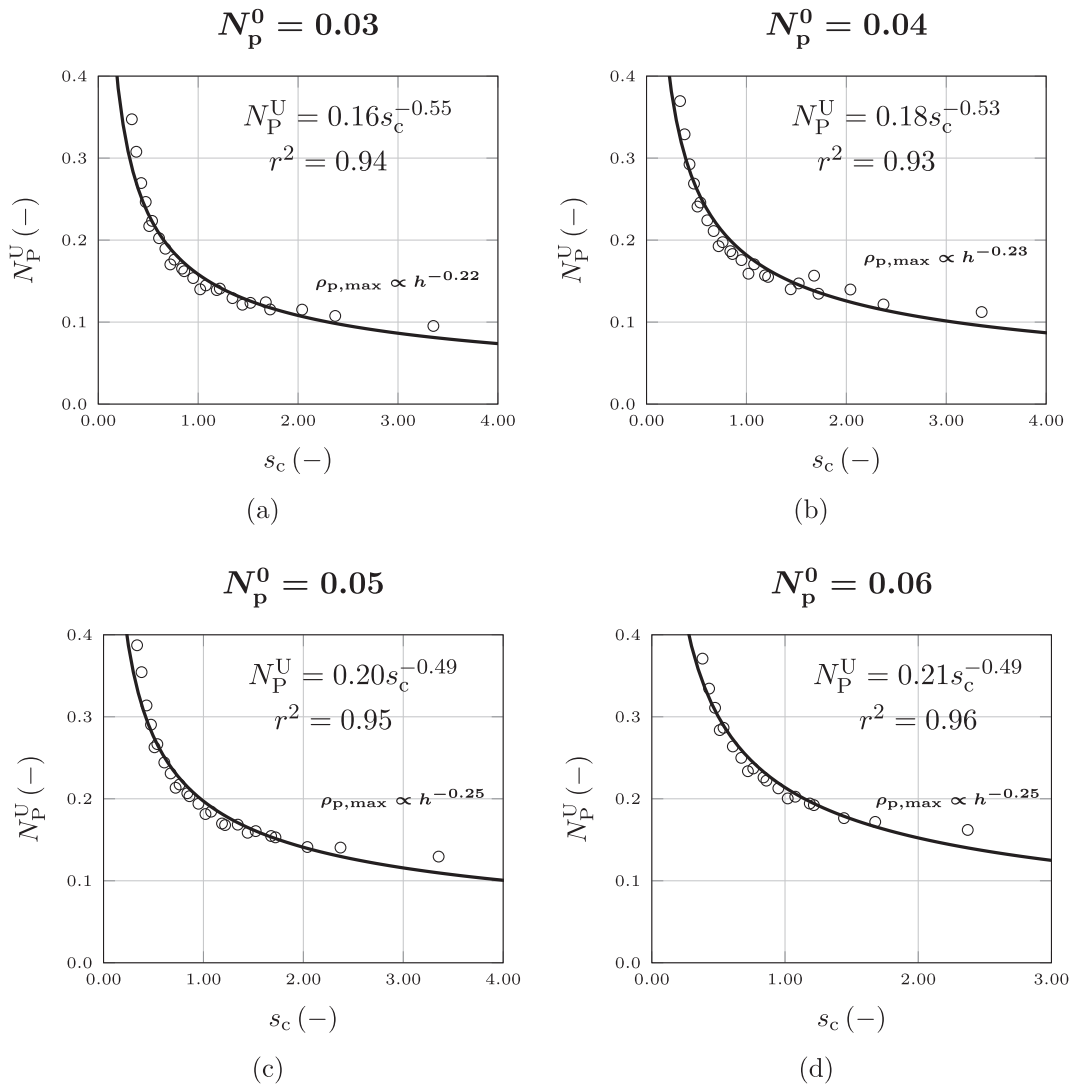

Fig. 12. Ductile-to-brittle transition in PC beams: (a) $N_p{}^0 = 0.03$; (b) $N_p{}^0 = 0.04$; (c) $N_p{}^0 = 0.05$; (d) $N_p{}^0 = 0.06$.

Concrete compressive strength, σ_c, is set as 40 MPa, whereas concrete tensile strength, σ_t, is set as 4 MPa. The critical value of crack opening, w^t_{cr}, is assumed as equal to 0.04 mm, whereas the critical overlapping as $w^c_{cr} = 1.5$ mm. In Fig. 10a, the nondimensional curves obtained for $\rho_p = 0.1\%$ are reported. It is possible to observe that all the beams present a ductile behavior: steel yielding develops after concrete cracking. Nevertheless, the extension of the plastic plateau decreases by increasing the beam depth, h. In Fig. 10b, the curves obtained for $\rho_p = 0.2\%$ are reported: it is possible to observe the same trend as for $\rho_p = 0.1\%$, although a more evident reduction in ductility (extension of plastic plateau) is registered. For steel percentages 0.4% and 0.8% (Fig. 10c and d), all the considered beams present a catastrophic behaviour: once the peak load is reached, a compressive snap-back is detected anticipating steel yielding.

4. Maximum reinforcement percentage in PC beams

As highlighted in the previous section, the nonlinear behaviour of PC beams can be described by several geometrical and mechanical parameters. It is possible to reduce the number of variables adopting a dimensional analysis approach [5,27,39]. The flexural behaviour of a PC beam can be represented as

$$M = \mathrm{F}\left(\sigma_t, G_F, \sigma_c, G_c, E, \sigma_y, \rho_p, \sigma_0, h; b/h, \ell/h, \vartheta\right) \tag{3}$$

E being the elastic modulus of concrete, σ_0 the stress generated at the beam extrados by the prestressing force, ℓ the beam span, and ϑ the plastic rotation of the cross-section.

If we focus our attention onto the maximum reinforcement percentage to avoid crushing failure ($\rho_{p,max}$), all the variables in Eq. (3) referring to concrete tensile behaviour can be neglected:

$$M = \mathrm{F}\left(\sigma_c, G_c, E, \sigma_y, \rho_p, \sigma_0, h; b/h, \ell/h, \vartheta\right) \tag{4}$$

Assuming as independent variables h and G_c, Eq. (4) leads to:

$$\frac{M}{\sqrt{G_c E} h^{2.5}} = \Pi\left(\frac{\sqrt{G_c E}}{\sigma_c h^{0.5}}, \rho_p \frac{\sigma_y h^{0.5}}{\sqrt{G_c E}}, \frac{\sigma_0 h^{0.5}}{\sqrt{G_c E}}, \vartheta \frac{\sqrt{G_c E}}{E h^{0.5}}\right) \tag{5}$$

Function F becomes Π because of the nondimensionalization given by Buckingham's Theorem [5,23,40]. For example, if the unit of measure of h changes, Π, being a dimensionless number, does not vary. Therefore, Π is not really a function of h nor of G_c. It is only a function of several dimensionless numbers, and thus it is possible to recognize the matrix brittleness number in compression, $s_c = (G_c E)^{0.5}/\sigma_c h^{0.5}$ [1,2], the reinforcement brittleness number, $N_P{}^U = \rho_p \sigma_y h^{0.5}/(G_c E)^{0.5}$ [40–42], as well as the prestressing brittleness number,

$$N_p^0 = \frac{\sigma_0 h^{0.5}}{\sqrt{G_c E}} = \sigma_p \frac{\rho_p h^{0.5}}{\sqrt{G_c E}} (6e/h - 1) \tag{6}$$

σ_p being the prestressing level in the steel strand and e its eccentricity with respect to the centre of gravity of the concrete section.

Therefore, a numerical study can be performed in order to determine the percentage $\rho_{p,max}$ based on the s_c-N_p^U diagram (for different values of $N^0{}_p$).

In Fig. 11, a parametric analysis for a PC beam with depth $h = 400$ mm, matrix brittleness number $s_c = 1.58$, and a prestressing brittleness number $N_p{}^0 = 0.05$ is reported. In Fig. 11a the beam exhibits a ductile behaviour since steel yielding occurs and a plastic plateau is detected: it corresponds to a stable condition with $\rho_p < \rho_{p,max}$. On the other hand, by increasing the steel percentage, the balanced condition can be obtained as in Fig. 11b: for $\rho_p = \rho_{p,max} = 0.42\%$, steel yielding and concrete crushing occur at the same time and the extension of the plastic plateau vanishes. The balanced condition reported in Fig. 11b corresponds to a reinforcement brittleness number $N_P{}^U = 0.15$ ($\sigma_y = 1700$ MPa, $G_c = 30$ N/mm, $E = 30000$ MPa). Finally, for $\rho_p > \rho_{p,max}$, i.e., when the balanced condition is overtaken, the beam presents a completely unstable condition since concrete crushing prevails and steel remains within the elastic range.

In the following, an extended parametric analysis is presented in order to outline a clear definition of over-reinforcement in PC beams. For each geometry, the reinforcement ratio has been modified until concrete crushing and steel yielding occur at the same time, i.e.,

$$w_r \approx w_y \tag{7}$$

being w_r the crack opening at the reinforcement level and w_y the crack opening generating steel yielding [27].

In Fig. 12, five different concrete grades and five different beam depths in the range $h = 0.2$–3.2 m are considered. In Fig. 12a and 12b, the results obtained for low prestressing levels, i.e., $N_p{}^0 = 0.03$ and $N_p{}^0 = 0.04$, are presented and a scale effect on $\rho_{p,max}$ is found proportional to $h^{-0.22}$ and $h^{-0.23}$, respectively. On the other hand, in Fig. 12c and 12d the cases $N_p{}^0 = 0.05$ and $N_p{}^0 = 0.06$ are reported. For this customary prestressing level ($\sigma_{p,max}/\sigma_y \approx 70\%$) a scale effect on $\rho_{p,max}$ proportional to $h^{-0.25}$ is obtained, providing the range in which PC structures can develop a safe ductile behavior [6,34].

5. Conclusions

In order to provide a comprehensive theoretical framework to prestressed concrete structural behavior, the correct definition of scale effects on the maximum reinforcement percentage requires a thorough knowledge of the complex phenomena characterizing tensile cracking and compression crushing failures. The Cohesive/Overlapping Crack Model presents a very high capability in predicting the post-cracking and post-crushing behaviour of prestressed concrete beams. The novelty of this model lies in the energy-based constitutive laws, which can describe the nonlinear phenomena involved in concrete cracking and crushing, together with their size-scale effects.

In the present work, a scale effect on maximum reinforcement percentage, ρ_{max}, is found proportional to $h^{-0.25}$, being h the beam depth. This condition can define the range in which prestressed concrete structures can develop a safe ductile behavior, giving the opportunity to formulate new standard requirements for an effective structural design.

CRediT authorship contribution statement

Alberto Carpinteri: Conceptualization, Formal analysis, Funding acquisition, Methodology, Project administration, Resources, Supervision, Validation, Writing – review & editing. **Federico Accornero:** Conceptualization, Formal analysis, Investigation, Methodology, Validation, Writing – original draft. **Renato Cafarelli:** Data curation, Software, Visualization, Writing – original draft.

Declaration of Competing Interest

The authors declare that they have no known competing financial interests or personal relationships that could have appeared to influence the work reported in this paper.

References

[1] Carpinteri A. Interpretation of the Griffith instability as a bifurcation of the global equilibrium. In: Shah SP, editor. Application of Fracture Mechanics to Cementitious Composites. Dordrecht: Springer Netherlands; 1985. p. 287–316. https://doi.org/10.1007/978-94-009-5121-1_10.

[2] Carpinteri A. Cusp catastrophe interpretation of fracture instability. J Mech Phys Solids 1989;37(5):567–82. https://doi.org/10.1016/0022-5096(89)90029-X.

[3] Biolzi L, Cangiano S, Tognon G, Carpinteri A. Snap-back softening instability in high strength concrete beams. Mater Struct (RILEM) 1989;22(6):429–36. https://doi.org/10.1007/BF02472220.

[4] Carpinteri A, Accornero F. Multiple snap-back instabilities in progressive microcracking coalescence. Eng Fract Mech 2018;187:272–81. https://doi.org/10.1016/j.engfracmech.2017.11.034.

[5] Carpinteri A. (1981). Size effect in fracture toughness testing: a dimensional analysis approach. Analytical and Experimental Fracture Mechanics (eds. G.C. Sih, M. Mirabile), Sijthoff & Noordhoff, Alphen aan den Rijn, The Netherlands, pp. 785-797.

[6] CEB Bulletin 242., 1998. Ductility of Reinforced Concrete Structures, Comité euro-international du Béton (CEB), Lusanne, Switzerland.

[7] Leonhardt F. Reducing the shear reinforcement in reinforced concrete beams and slabs. Mag Concr Res 1965;17(53):187–98. https://doi.org/10.1680/macr.1965.17.53.187.

[8] Kani GNJ. How safe are our large reinforced concrete beams? Struct J (ACI) 1967;64(3):128–41.

[9] Tan KH, Lu HY, Teng S. Size effects in large prestressed concrete deep beams. Struct J (ACI) 1999;96(6):937–46.

[10] Vorel J, Gattu M, Bažant ZP. Size effect in flexure of prestressed concrete beams failing by compression softening. J Struct Eng (ASCE) 2014;140(10):04014068. https://doi.org/10.1061/(ASCE)ST.1943-541X.0000983.

[11] Belgin CM, Sener S. Size effect on failure of overreinforced concrete beams. Eng Fract Mech 2008;75(8):2308–19. https://doi.org/10.1016/j.engfracmech.2007.09.006.

[12] Bažant ZP. Size effect in blunt fracture: concrete, rock, metal. J Eng Mech (ASCE) 1984;110(4):518–35. https://doi.org/10.1061/(ASCE)0733-9399(1984)110:4(518).

[13] ACI Committee 446 (1992). ACI PRC-446.1-91: Fracture Mechanics of concrete: concepts; models and determination of material properties (ed. Z. P. Bažant), Elsevier, London, (UK).

[14] Kim J-K, Yi S-T. Application of size effect to compressive strength of concrete members. Sadhana 2002;27(4):467–84.

[15] Yi S-T, Kim M-S, Kim J-K, Kim J-H-J. Effect of specimen size on flexural compressive strength of reinforced concrete members. Cem Concr Compos 2007;29(3):230–40. https://doi.org/10.1016/j.cemconcomp.2006.11.005.

[16] Carpinteri A. Notch sensitivity in fracture testing of aggregative materials. Eng Fract Mech 1982;16(4):467–81. https://doi.org/10.1016/0013-7944(82)90127-8.

[17] Wittmann FH, Rokugo K, Brühwiler E, Mihashi H, Simonin P. Fracture energy and strain softening of concrete as determined by means of compact tension specimens. Mater Struct 1988;21(1):21–32. https://doi.org/10.1007/BF02472525.

[18] Hillerborg A, Modéer M, Petersson P-E. Analysis of crack formation and crack growth in concrete by means of fracture mechanics and finite elements. Cem Concr Res 1976;6(6):773–81. https://doi.org/10.1016/0008-8846(76)90007-7.

[19] Gopalaratnam VS, Shah SP. Softening response of plain concrete in direct tension. Structural Journal (ACI) 1985;82:310–23.

[20] van Vliet MRA. Size effect in tensile fracture of concrete and rock. Delft, The Netherlands: Technical University of Delft; 2000. PhD Thesis.

[21] van Mier JGM, Shah SP, Arnaud M, Balayssac JP, Bascoul A, Choi S, et al. Strain-softening of concrete in uniaxial compression. Mater Struct 1997;30(4):195–209. https://doi.org/10.1007/BF02486177.

[22] Ferrara G, Gobbi ME. Strain softening of concrete under compression. Report to RILEM Committee 148. 1995.

[23] Jansen DC, Shah SP. Effect of length on compressive strain softening of concrete. J Eng Mech (ASCE) 1997;123(1):25–35. https://doi.org/10.1061/(ASCE)0733-9399(1997)123:1(25).

[24] Carpinteri A, Corrado M, Mancini G, Paggi M. Size-scale effects on plastic rotational capacity of reinforced concrete beams· Struct J (ACI) 2009;106:887–96.

[25] Accornero F, Cafarelli R, Carpinteri A. Cracking and crushing in prestressed concrete beams· Struct J (ACI) 2021;118(2):101–9.

[26] Accornero F, Cafarelli R, Carpinteri A. The Cohesive/Overlapping Crack Model for plain and RC beams: scale effects on cracking and crushing failures· Mag Concr Res 2021. https://doi.org/10.1680/jmacr.20.00260.

[27] Carpinteri A, Accornero F, Cafarelli R. Scale-dependent maximum reinforcement percentage in reinforced concrete beams· Struct Concrete (*fib*) 2021;22(4):2155–66. https://doi.org/10.1002/suco.202000573.

[28] Bocca P, Carpinteri A, Valente S. Mixed mode fracture of concrete. Int J Solids Struct 1991;27(9):1139–53. https://doi.org/10.1016/0020-7683(91)90115-V.

[29] Hawkins N.M., Hjorteset K. (1992). Minimum reinforcement requirements for concrete flexural members. Applications of Fracture Mechanics to Reinforced Concrete (ed. A. Carpinteri), Elsevier, London, UK, pp. 379-412.
[30] Ruiz G., Elices M., Planas J. (1999). Size Effect and Bond-Slip Dependance of Lightly Reinforced Concrete Beams. Minimum Reinforcement in Concrete Members (ed. A. Carpinteri), Elsevier, Oxford, UK, pp. 67-97.
[31] Hillerborg A. Results of three comparative test series for determining the fracture energy G_F of concrete. Mater Struct 1985;18(5):407–13. https://doi.org/10.1007/BF02472416.
[32] Carpinteri A, Corrado M, Mancini G, Paggi M. The overlapping crack model for uniaxial and eccentric concrete compression tests. Mag Concr Res 2015;61(9):745–57. https://doi.org/10.1680/macr.2008.61.9.745.
[33] fib (Fédération Internationale du Béton). Model Code for Concrete Structures 2010. New York, New York, USA: John Wiley & Sons; 2013.
[34] AASHTO, 2019. LRFD Minimum Flexural Reinforcement Requirements. National Cooperative Highway Research Program (NCHRP) Research Report 906.
[35] Naaman AE, Muhamed HH, Wright JK. Analysis of ductility in partially prestressed concrete flexural members. Prestressed Concrete Inst J 1986;31(3):64–87. https://doi.org/10.15554/pcij.05011986.64.87.
[36] Warvaruk J, Sozen MA, Siess CP. Strength and behavior in flexure of prestressed concrete beams. Illinois, USA: University of Illinois; 1962.
[37] Billet D.F. (1953). Study of prestressed concrete beams failing in flexure. University of Illinois, MSC Thesis, Illinois, USA.
[38] Suzuki M., Akiyama M., Matsuzaki H., Dang T.H. (2006). Concentric loading test of RC columns with normal and high-strength materials and averaged stress-strain model for confined concrete considering compressive fracture energy. Proceedings of the Second International fib Congress, Doppiavoce, Naples, Italy.
[39] Carpinteri A, Accornero F. Dimensional analysis of critical phenomena: self-weight failure, turbulence, resonance, fracture. Phys Mesomech 2020;24(4):111–6. https://doi.org/10.24411/1683-805X-2020-16008.
[40] Carpinteri A. A fracture mechanics model for reinforced concrete collapse. Proceedings of the IABSE Colloquium on Advanced Mechanics of Reinforced Concrete. Delft, The Netherlands: Delft University Press; 1981. p. 17–30.
[41] Carpinteri A. Stability of fracturing process in RC beams. J Struct Eng (ASCE) 1984;110(3):544–58. https://doi.org/10.1061/(ASCE)0733-9445(1984)110:3(544).
[42] Carpinteri A, Accornero F. The Bridged Crack model with multiple fibers: local instabilities, scale effects, plastic shake-down, and hysteresis. Theor Appl Fract Mech 2019;104:102351. https://doi.org/10.1016/j.tafmec.2019.102351.